

RESEARCH ARTICLE

10.1002/2016JD024758

Key Points:

- Dust concentration over eastern China has significant negative correlation to the East Asian Monsoon index (EAMI)
- Dust concentrations between the weakest and strongest EAM years differ by 55.6% in eastern China
- With fixed emissions, transport and removal processes contribute 60% to the total difference in dust over eastern China

Supporting Information:

- Supporting Information S1

Correspondence to:

L. M. Russell,
lmrussell@ucsd.edu

Citation:

Lou, S., L. M. Russell, Y. Yang, L. Xu, M. A. Lamjiri, M. J. DeFlorio, A. J. Miller, S. J. Ghan, Y. Liu, and B. Singh (2016), Impacts of the East Asian Monsoon on springtime dust concentrations over China, *J. Geophys. Res. Atmos.*, 121, 8137–8152, doi:10.1002/2016JD024758.

Received 4 JAN 2016

Accepted 24 JUN 2016

Accepted article online 27 JUN 2016

Published online 12 JUL 2016

Impacts of the East Asian Monsoon on springtime dust concentrations over China

Sijia Lou^{1,2}, Lynn M. Russell¹, Yang Yang^{1,2}, Li Xu¹, Maryam A. Lamjiri¹, Michael J. DeFlorio¹, Arthur J. Miller¹, Steven J. Ghan², Ying Liu², and Balwinder Singh²

¹Scripps Institution of Oceanography, University of California, San Diego, La Jolla, California, USA, ²Now at Atmospheric Science and Global Change Division, Pacific Northwest National Laboratory, Richland, Washington, USA

Abstract We use 150 year preindustrial simulations of the Community Earth System Model to quantify the impacts of the East Asian Monsoon strength on interannual variations of springtime dust concentrations over China. The simulated interannual variations in March–April–May (MAM) dust column concentrations range between 20–40% and 10–60% over eastern and western China, respectively. The dust concentrations over eastern China correlate negatively with the East Asian Monsoon (EAM) index, which represents the strength of monsoon, with a regionally averaged correlation coefficient of -0.64 . Relative to the strongest EAM years, MAM dust concentrations in the weakest EAM years are higher over China, with regional relative differences of 55.6%, 29.6%, and 13.9% in the run with emissions calculated interactively and of 33.8%, 10.3%, and 8.2% over eastern, central, and western China, respectively, in the run with prescribed emissions. Both interactive run and prescribed emission run show the similar pattern of climate change between the weakest and strongest EAM years. Strong anomalous northwesterly and westerly winds over the Gobi and Taklamakan deserts during the weakest EAM years result in larger transport fluxes, and thereby increase the dust concentrations over China. These differences in dust concentrations between the weakest and strongest EAM years (weakest–strongest) lead to the change in the net radiative forcing by up to -8 and -3 W m^{-2} at the surface, compared to -2.4 and $+1.2$ W m^{-2} at the top of the atmosphere over eastern and western China, respectively.

1. Introduction

Dust is a prominent atmospheric aerosol that adversely affects human health, air quality, and atmospheric visibility. Through scattering and absorbing shortwave (SW) and longwave (LW) radiation, dust can also change the Earth's energy balance [Carlson and Benjamin, 1980; Sokolik and Toon, 1996] and hence influence the climate [Ahn et al., 2007; Jin et al., 2014; Bangalath and Stenchikov, 2015]. Asian dust mainly originates in the arid and semiarid regions in northwestern China and deserts of Mongolia, with the largest production during spring [Chen et al., 1999; Merrill et al., 1989; Sun et al., 2001; Xuan and Sokolik, 2002; Zhang et al., 1996, 1997, 1998, 2003; Prijith et al., 2013]. Mineral dust is then transported over the Asian continent by northwesterly winds near the surface and over the Pacific Ocean by westerly winds in the free troposphere [Duce et al., 1980; Holzer et al., 2003; Husar et al., 1997, 2001; Uematsu et al., 1983; Uno et al., 2003]. High concentrations of dust have been observed over many locations in China, with monthly mean concentrations of 30–200 and 200–400 $\mu\text{g m}^{-3}$ in spring over eastern and western China, respectively, with episodic dust concentrations exceeding 500 and 1000 $\mu\text{g m}^{-3}$ [Wang et al., 2008; Li and Zhang, 2012; X. Y. Zhang et al., 2012].

Previous observational and modeling studies have shown that variations in winds, temperature, soil moisture, and precipitation can influence dust emissions, transport, and deposition, as well as dust concentrations in East Asia [Xuan and Sokolik, 2002; Wang et al., 2004; Gong et al., 2006; Hara et al., 2006; Kimura, 2012; Tan et al., 2012; Abulaiti et al., 2014] and in other parts of the world [e.g., Doherty et al., 2014; DeFlorio et al., 2015]. The interannual variation of winds is known to be the most important factor that influences dust concentrations over China. Hara et al. [2006] reported that the variation of dust days in the Gobi desert region was controlled by the frequency of strong winds, based on the Regional Atmospheric Modeling System/Chemical weather Forecasting System and visibility observations by Chinese and Japanese Meteorological Agencies during spring from 1972 to 2004. Gong et al. [2006] analyzed the interannual variability of spring Asian dust emissions, concentrations, deposition, transport, and budgets over the period of 1960 to 2003 using the Northern Aerosol Regional Climate Model. They found that surface wind speed has a more significant impact on dust production than precipitation and surface temperature. For other factors,

previous studies suggested that the regional dust storms in northern China are negatively correlated with prior winter temperature [Qian *et al.*, 2004]. While precipitation reduces dust emissions mainly through suppressing emission when snow covers the potential dust source areas and increasing soil moisture when snow melts [Tanaka *et al.*, 2011; Lee and Kim, 2012], precipitation also reduces dust emissions in other seasons by impacting soil moisture and vegetation conditions over dust source regions [Liu *et al.*, 2004].

Spring winds show significant interannual variations over China [Zhao *et al.*, 2007; Guo *et al.*, 2011], which are partially associated with the East Asian Monsoon (EAM). Gong *et al.* [2006] pointed out that the strength of the East Asian Monsoon could not influence the dust production directly but could impact the dust transport. Yumimoto and Takemura [2015] found that the dust outflow was negatively correlated with the East Asian Monsoon index (EAMI). These previous studies have not systematically examined the impacts of the EAM strength on interannual variations of springtime dust in China.

The interannual variations of dust can further influence the clear-sky radiative energy budget. Mineral dust reduces the downward shortwave radiation at the surface through scattering and absorption of solar flux [Miller and Tegen, 1998; Ahn *et al.*, 2007; Shell and Somerville, 2007; Park *et al.*, 2010], while the impact of dust on solar radiation in the upper troposphere depends on the regional albedo [Liao and Seinfeld, 1998; Satheesh *et al.*, 2007; Yue *et al.*, 2010]. Dust longwave radiative forcing was found to increase the downward radiative flux at the surface [Cautenet *et al.*, 1991; Markowicz *et al.*, 2003] and reduce the outgoing radiative flux at the top of the atmosphere [Ackerman and Chung, 1992; Haywood *et al.*, 2005]. The net radiative forcing over China is in the range of -5 to -15 W m^{-2} at the surface and -5 to $+5 \text{ W m}^{-2}$ at the top of the atmosphere (TOA) during spring [Zhang *et al.*, 2009], with a smaller annual radiative forcing of -1 to -10 W m^{-2} and -3 to $+2 \text{ W m}^{-2}$, respectively [Yue *et al.*, 2010; Zhao *et al.*, 2013].

The studies cited above were not able to isolate the effects of the EAM on Asian dust because causality could not be demonstrated. The goal of this study is to systematically isolate the EAM impacts of wind fields on dust concentrations over China using the Community Earth System Model (CESM). Considering the wind variation as an annual cycle, we use a unified East Asian Monsoon index (EAMI) [Li and Zeng, 2002] to examine the interannual variations in wind field that result from the competition between East Asian winter and summer monsoon in spring. The EAM strength thus serves as a useful metric for the interannual variations of dust concentrations and radiative effects in spring. The model description, numerical experiments, and method for calculating EAMI are described in section 2. Section 3 presents simulated impacts of EAM strength on interannual variations of dust concentrations, and section 4 examines the influence of changes in dust concentrations on radiative forcing.

2. Method

2.1. Model Description

We simulate preindustrial conditions for 150 years using the Community Earth System Model (CESM), which is composed of atmosphere, ocean, land surface, and sea ice components [Hurrell *et al.*, 2013]. The atmospheric model has a horizontal resolution of 1.9° latitude by 2.5° longitude and 30 vertical layers from the surface to 3.6 hPa. The ocean component using the Parallel Ocean Program version 2 [Smith *et al.*, 2010] is coupled with a three-dimensional active model. CESM includes the properties and processes of aerosol species (sulfate, black carbon, primary organic matter, secondary organic matter, sea salt, and mineral dust) in the modal aerosol module [Liu *et al.*, 2012]. The aerosol size distribution is represented by a trimodal lognormal distribution for Aitken, accumulation, and coarse modes. The optical properties of aerosols are calculated as described in Ghan and Zaveri [2007].

Mineral dust is emitted in both accumulation ($0.1\text{--}1 \mu\text{m}$) and coarse ($1\text{--}10 \mu\text{m}$) modes following the treatment of Zender *et al.* [2003]. Within a single mode, dust is assumed to be internally mixed with other aerosol species. The bulk hygroscopicity and refractive index are calculated by volume-weighting hygroscopicities and refractive indices of each individual aerosol species. Solar absorption by dust aerosol is enhanced by coatings of sulfate, organics, and water. The hygroscopicity of mineral dust is assumed to be 0.068, while the dust refractive indices are obtained from Optical Properties of Aerosols and Clouds (OPAC) [Hess *et al.*,

1998]. Dust is transported by the vertical diffusion, resolved winds, and cumulus mass flux, as well as removed by dry deposition, nucleation scavenging, and impact ion scavenging schemes in CAM5 as described by Liu *et al.* [2012].

2.2. 150 Year Simulations in Preindustrial Conditions

To identify the relative importance of variations in emission, transport, and deposition that influence dust concentrations in different dynamical normalized seasonality monsoon years, we perform the following simulations:

1. IRUN: The standard simulation for preindustrial conditions (all the greenhouse gases and anthropogenic aerosol emissions are fixed at the level of the year 1850) uses interactive emissions and removal.
2. PRUN: Same as the IRUN simulation but with prescribed emissions for dust aerosols. Emissions of dust aerosol are fixed to climatological monthly mean values of IRUN, which therefore eliminates interannual variability of dust emissions in this simulation.

All simulations are initialized from a previous CESM simulation of 221 years with 1850 emissions, and no changes other than prescribed emissions are introduced. Simulated global mean surface temperature fluctuated between 276.2 K and 277.2 K during the 150 year simulation (Figure S1 in the supporting information), reaching an equilibrium state. From the time series it is clear that the adjustment period at the start of the simulation is quite short, namely, only a few years. Comparing results from these two simulations will reveal the influence of interannual variations in emissions on the simulated dust distributions.

2.3. The Calculation of East Asian Monsoon Index (EAMI)

Due to the strong seasonal variation in wind over East Asia resulting from the monsoons [Webster and Yang, 1992], we use the East Asian Monsoon index (EAMI) to quantify the variations in wind fields, which is defined by Li and Zeng [2002]. This index is based on the seasonal mean intensity of wind fields and has been adopted as the real-time monsoon index for East Asia by the National Oceanic and Atmospheric Administration (NOAA, http://www.cpc.ncep.noaa.gov/products/Global_Monsoons/Asian_Monsoons/monsoon_index.shtml). The index is also intensively used in analyzing ozone and aerosols [He *et al.*, 2008; Zhu *et al.*, 2012; Zhou *et al.*, 2013]. Since spring is the transitional season between the East Asian winter and summer monsoon, the wind field over northeastern China is dominated by northwesterlies in the lower troposphere during the winter monsoon [Zhou, 2011], while over southeastern China it is dominated by southwesterlies during the summer monsoon [Yang *et al.*, 2014]. The competition between northwesterly and southwesterly winds impacts the dust emission and transport, indicating that changes in transfer winds play an important role in affecting interannual variations of dust concentrations.

For a given grid point (i, j) and pressure level, the EAMI on the m th month of the n th year is formulated as

$$\delta_{nm}(i, j) = \frac{\|\bar{V}_w(i, j) - V_{nm}(i, j)\|}{\|\bar{V}(i, j)\|} - 2 \quad (1)$$

where \bar{V}_w is the climatological mean wind vector in winter, V_{nm} is the monthly wind vector on the m th month of the n th year (here we use the mean of March–April–May for each year in the Northern Hemisphere and September–October–November in the Southern Hemisphere to represent spring), and $\bar{V} = (\bar{V}_w + \bar{V}_s)/2$ is the climatological mean wind vector, where \bar{V}_s is the climatological mean wind vector in summer. We assume $\bar{V}_w = \bar{V}_{\text{January}}$ and $\bar{V}_s = \bar{V}_{\text{July}}$ in the Northern Hemisphere, whereas $\bar{V}_w = \bar{V}_{\text{July}}$ and $\bar{V}_s = \bar{V}_{\text{January}}$ in the Southern Hemisphere. According to Li and Zeng [2002], the value 2 in formula (1) is the critical value of significance of the quantity. In the Northern Hemisphere, for example, $\delta < 0$ (or $\delta > 0$) represents the angle between V_{nm} and V_w less than (or larger than) 90° and characterized as winter (or summer) monsoon.

The CESM long-term simulation of temperature, precipitation, and wind fields is similar to National Center for Atmospheric Research/National Centers for Environmental Prediction (NCAR/NCEP) reanalyses (Figure S2) [Small *et al.*, 2014; Wang *et al.*, 2015]. The CESM interannual variations of temperature, precipitation, and wind fields in the same simulation [Yang *et al.*, 2016a, 2016b] provide an illustration of the interannual variations in EAM strength. The modeled EAMI is calculated from wind fields at the pressure level of 850 hPa using the 150 year simulations of IRUN and PRUN. We also calculate the EAMI using the NCEP/NCAR reanalysis data sets

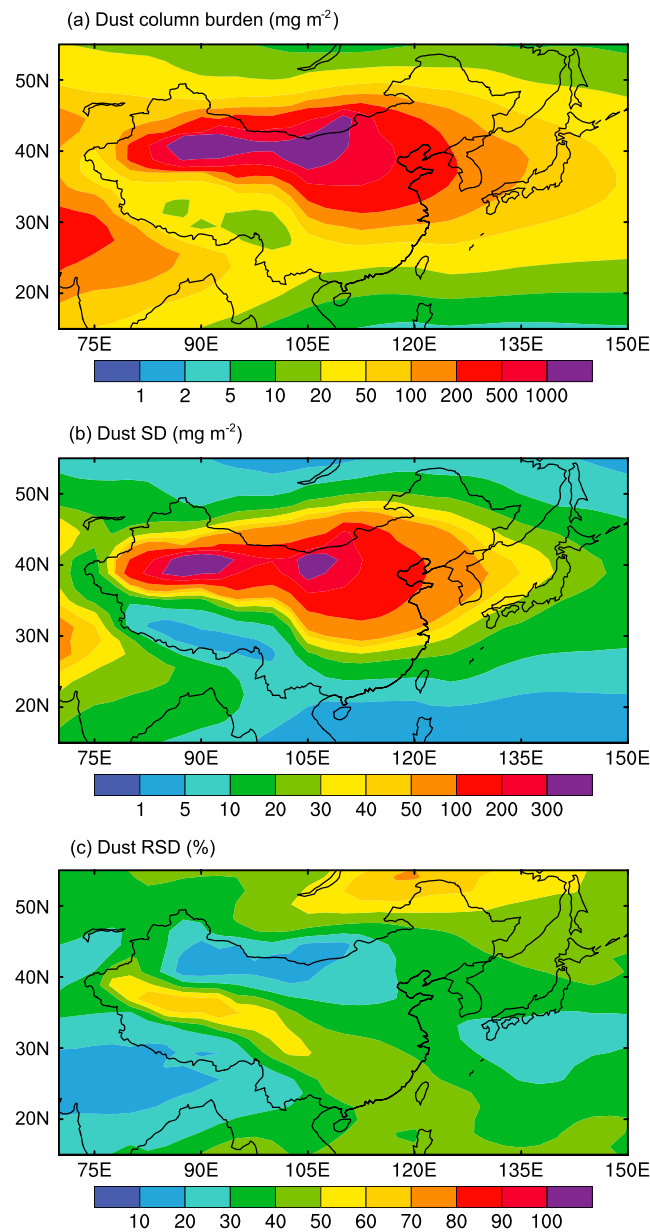


Figure 1. (a) Simulated MAM dust column burden (mg m^{-2}) averaged over 150 year IRUN simulation. (b) Standard deviation (SD, mg m^{-2}) and (c) relative standard deviation (RSD, %) calculated for 150 year IRUN simulation.

desert [Zhao *et al.*, 2006]. It should be noted that the dust concentrations in preindustrial conditions are larger than those in the current climate. The simulated climatological annual mean surface-layer dust concentrations in IRUN are 37% higher than observations compared to the measurements taken at 15 sites over a large fraction of China during the period of 2006–2007 from X. Y. Zhang *et al.* [2012] (Figure S4). This result agrees with Mahowald *et al.* [2006a, 2006b], who suggested that the globally averaged dust loadings in preindustrial conditions are 31% larger than current conditions, due to the changes in dust source regions associated with vegetation, precipitation, temperature, and cloudiness.

Figures 1b and 1c show the standard deviation (SD) and relative standard deviation (RSD) of dust column burden during springtime. The pattern of SD of dust burden is similar to the climatological mean spatial distribution of dust, with higher SD values associated with the higher mean dust burden. The largest values exceed

during the period from 1948 to 2014 for comparison. Negative values of EAMI represent the winter monsoon, indicating weak EAM years, while positive values represent the summer monsoon, indicating strong EAM years. Physically, weak (or strong) EAM over China during springtime is characterized by strong (or weak) westerlies and northerlies over north China and by weak (or strong) southerlies over south China.

3. Results

3.1. Simulated Interannual Variations of Springtime Dust in China

Figure 1a shows the climatological mean spatial distribution of March-April-May (MAM) dust column burden southeast Asia from the 150 year IRUN simulation. Simulated dust burden exhibits a maximum value up to 1000 mg m^{-2} in western China, around the dust source regions in Gobi and Taklamakan deserts. The high dust concentrations in western and central China are consistent with previous observations and modeling studies [Gong *et al.*, 2003; Wang *et al.*, 2004, 2008; Zhao *et al.*, 2006; Zhang and Liao, 2016]. Over eastern China, simulated dust burden values are $200\text{--}1000 \text{ mg m}^{-2}$ in northeastern China and $20\text{--}200 \text{ mg m}^{-2}$ in southeastern China, with a surface-layer (the lowest atmospheric layer in the model) dust concentration of $50\text{--}300$ and $5\text{--}50 \mu\text{g m}^{-3}$ (Figure S3). This pattern of higher dust concentrations in northeastern China relative to southeastern China is a result of the regional-scale transport dominated by surface level northwesterly winds associated with the East Asian winter monsoon from the Gobi

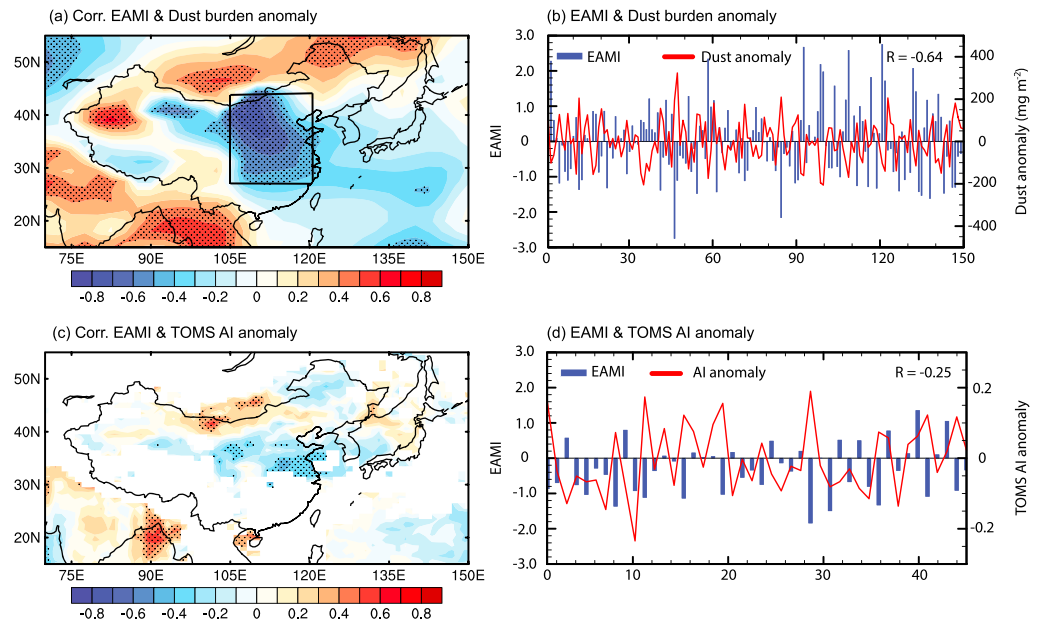


Figure 2. (a) Spatial distribution of the correlation coefficients between the EAMI and the dust burden anomaly in MAM both calculated from IRUN and (c) the EAMI calculated from NCEP/NCAR reanalysis data sets and the TOMS AI anomaly. The dotted areas indicate statistical significance with 95% (P value < 0.05) from a two-tailed Student's t test. The normalized time series of EAMI (blue bars, left y axis) and (b) the simulated averaged MAM dust burden anomaly (red line, right y axis, mg m^{-2}) for 150 year simulations and (d) EAMI from NCEP/NCAR reanalysis data sets and averaged monthly TOMS AI anomaly (red line, right y axis) in spring for years of 1979–1993.

300 mg m^{-2} over the Gobi and Taklamakan deserts. SD and RSD values of dust burden are in the range of $50\text{--}200 \text{ mg m}^{-2}$ and $20\text{--}40\%$ over northeastern China (north of 35°N) and $5\text{--}50 \text{ mg m}^{-2}$ and $30\text{--}50\%$ over southeastern China (south of 35°N), respectively. These interannual variations of dust concentrations in eastern China are significant compared to the changes in aerosol concentrations caused by anthropogenic activities. For example, *Yang et al.* [2015] showed the outflow fluxes of sulfate from East Asia increased by up to 50% due to both changes in meteorology and increased SO_2 emission (up to 100%) from 1986 to 2006.

3.2. Impacts of the EAM on Interannual Variations of Springtime Dust in China

In order to investigate the interannual variability of springtime wind field and its impact on dust aerosol concentrations in China, we calculated the correlation coefficients between local EAMI and dust burden during March–April–May for the 150 year interactive simulation (IRUN). As shown in Figure 2a, the simulated dust burden anomaly correlates negatively with the EAMI over a large fraction of China, with maximum negative correlation coefficients up to -0.7 over central China around the Gobi desert and with weak positive correlations up to 0.5 over central Mongolia and the Taklamakan desert. Over central and eastern China ($105^\circ\text{E}\text{--}120^\circ\text{E}$, $25^\circ\text{N}\text{--}45^\circ\text{N}$), the averaged correlation coefficient is -0.64 , which is statistically significant with 95% confidence (P value < 0.05). This region with the largest negative correlation (black box in Figure 2a) is chosen to calculate the averaged EAMI; the bars in Figure 2b are the time series of the normalized EAMI, which represent the interannual variation of the strength of the EAM. A similar pattern was found in Figure 2c when we calculated the correlation coefficients between EAMI (based on the NCEP reanalysis data) and TOMS AI (Total Ozone Mapping Spectrometer Aerosol Index) anomaly, with a smaller averaged correlation coefficient value of -0.25 over central and eastern China (Figure 2d) and $+0.2$ over Mongolia. The difference between simulated and observed values may be partly due to the contribution from anthropogenic aerosols, such as black carbon and brown carbon, which also contributes to AI values [*Wang*, 2013]. Although we choose the period between 1979 and 1993, which contained low anthropogenic emissions in China, the concentrations of black carbon and brown carbon in these years are still much higher than the preindustrial period that we simulated in this study. The negative correlation coefficient between the dust transport flux over the western Pacific and EAMI is also reported by *Yumimoto and Takemura* [2015], consistent with our results.

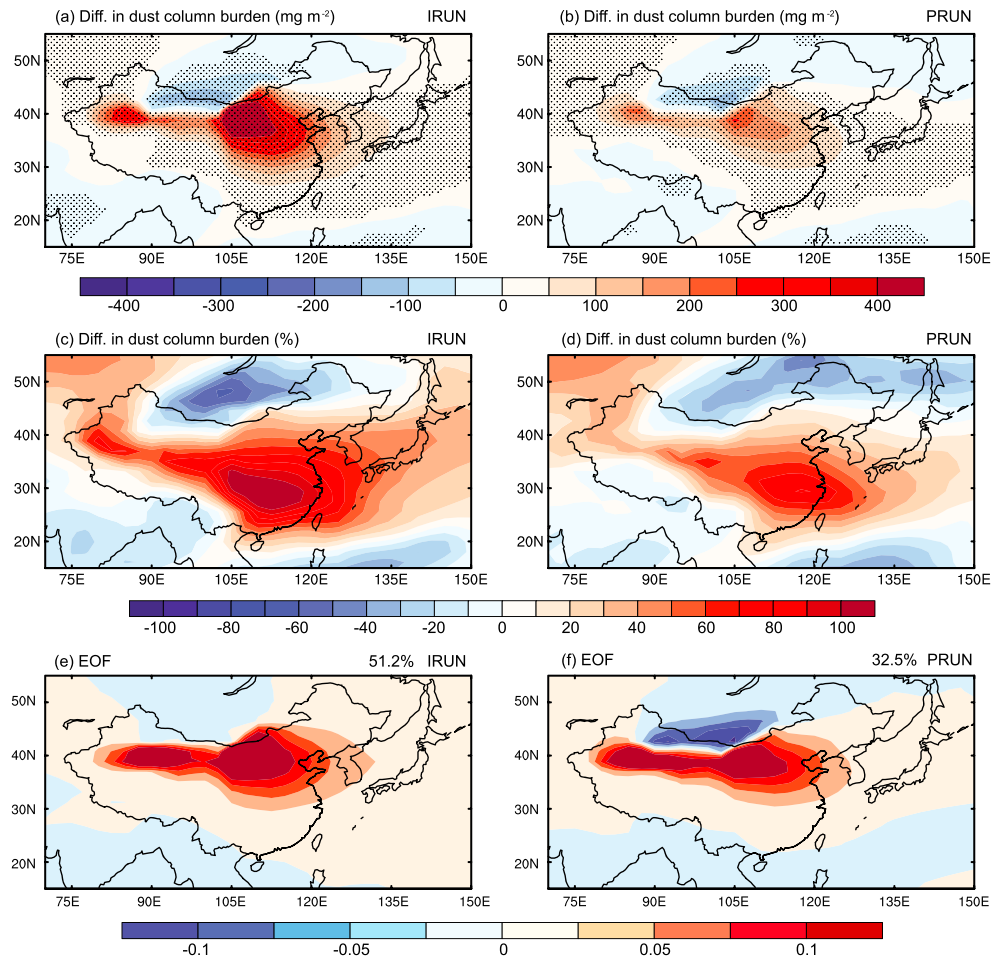


Figure 3. Horizontal distributions of (a and b) absolute and (c and d) percentage differences in MAM dust column burden between the weakest and strongest EAM years (weakest–strongest). (e and f) The leading mode EOF of spring anomalies of dust column burden, with the variance explained by the leading mode EOF given at the upper right corner of the bottom plot. Results of the left and right column are from IRUN and PRUN simulations, respectively, and the units used are shown on top of each panel. The dotted areas indicate statistical significance with 95% (P value < 0.05) from a two-tailed Student’s t test.

In order to quantify the impacts of EAM on dust concentrations over China, the absolute and percentage differences between dust column burden averaged over the 10% weakest EAM years and those averaged over the 10% strongest EAM years (follows the definition of extreme events from *Intergovernmental Panel on Climate Change* [2013]) from IRUN simulation are calculated and shown in Figures 3a and 3c, respectively. The weakest (or strongest) EAM years are selected within the 150 year simulation based on the 15 most negative (or positive) values of the normalized EAMI over eastern China as shown in Figure 2a. Relative to the strongest EAM years, the dust column burden in the weakest EAM years is higher over a large fraction of China, with the maximum value exceeding 300 mg m^{-2} over northern China around the high dust source regions, and is slightly lower over Mongolia. Over eastern China ($110^{\circ}\text{E}–120^{\circ}\text{E}$, $20^{\circ}\text{N}–45^{\circ}\text{N}$), the simulated dust column burden averaged in the weakest EAM years is higher than that averaged in the strongest EAM years by $50–250 \text{ mg m}^{-2}$ (or 30–80%), with an averaged value of 171.0 mg m^{-2} (or 54.1%).

We also use an empirical orthogonal function (EOF) analysis of monthly anomalies of the simulated MAM dust column burden to explore the interannual variations of spring dust burden from IRUN. The EOF analysis is often used to reveal independent spatiotemporal modes of variability of a particular data field. The leading EOF mode, which explains the largest variance of dust burden in MAM from IRUN, represents 51.2% of the interannual variations of the simulated spring dust (Figure 3e). The leading EOF of dust in MAM shows a positive pattern over the eastern and northern China but displays a weak negative pattern over Mongolia.

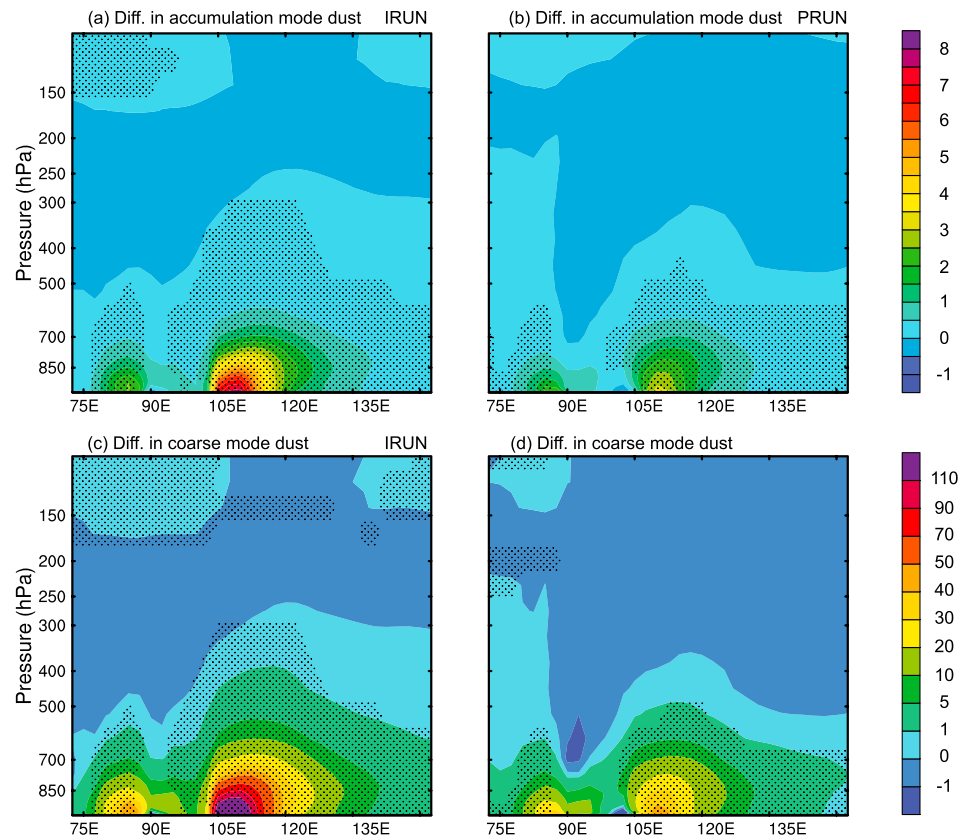


Figure 4. Pressure-longitude cross sections averaged over 25–45°N for absolute differences in (a and b) accumulation mode and (c and d) coarse mode of dust concentrations in MAM between the weakest and strongest EAM years (weakest-strongest). Results of the left and right column are from IRUN and PRUN simulations, respectively, and the units are $\mu\text{g m}^{-3}$. The dotted areas indicate statistical significance with 95% (P value < 0.05) from a two-tailed Student's t test.

A similar pattern was found from the difference in dust between the weakest and strongest EAM years (Figure 3a). The correlation coefficient between the leading EOF principal component and normalized EAM over central and eastern China is found to be -0.54 , indicating that the changes in wind field dominate the interannual variations of dust in MAM.

Figures 3b and 3d show the absolute and percentage differences between dust column burden averaged over the 10% weakest EAM years and those averaged over the 10% strongest EAM years from PRUN simulation, respectively. The averaged differences in dust column burden for PRUN between the weakest and strongest EAM years are simulated to be 67.9 mg m^{-2} (or 32.5%) over eastern China, due to contributions from transport from dust source regions. A similar pattern of differences in dust column burden was found when the dust emission was fixed in PRUN, indicating the sensitivity of interannual variations of dust to wind direction. The leading EOF of spring dust burden in PRUN explains 32.5% of interannual variations, with a positive pattern over eastern and northern China, and a strong negative pattern over Mongolia (Figure 3b).

To see the vertical distribution of the EAM influence on dust, Figure 4 presents pressure-longitude plots of the differences (weakest-strongest EAM) in accumulation (Figures 4a and 4b) and coarse (Figures 4c and 4d) mode dust concentration averaged over the latitude range 25–45°N from the IRUN and PRUN simulations. As shown in Figures 4a and 4c, dust concentrations of accumulation mode and coarse mode in the weakest EAM years are higher by up to 7 and $110 \mu\text{g m}^{-3}$, respectively, over 105–110°E near the surface of the major Asian dust sources (Figure 5c) and by up to 3 and $30 \mu\text{g m}^{-3}$ over 120–125°E further away from high dust source regions at 850 hPa, relative to the concentrations in the strongest EAM years. Figures 4b and 4d show a similar pattern but with smaller values of 2–3.5 and $20\text{--}40 \mu\text{g m}^{-3}$ over 105–110°E and of 1–2 and $10\text{--}20 \mu\text{g m}^{-3}$ over 120–125°E, respectively. Considering the fixed dust

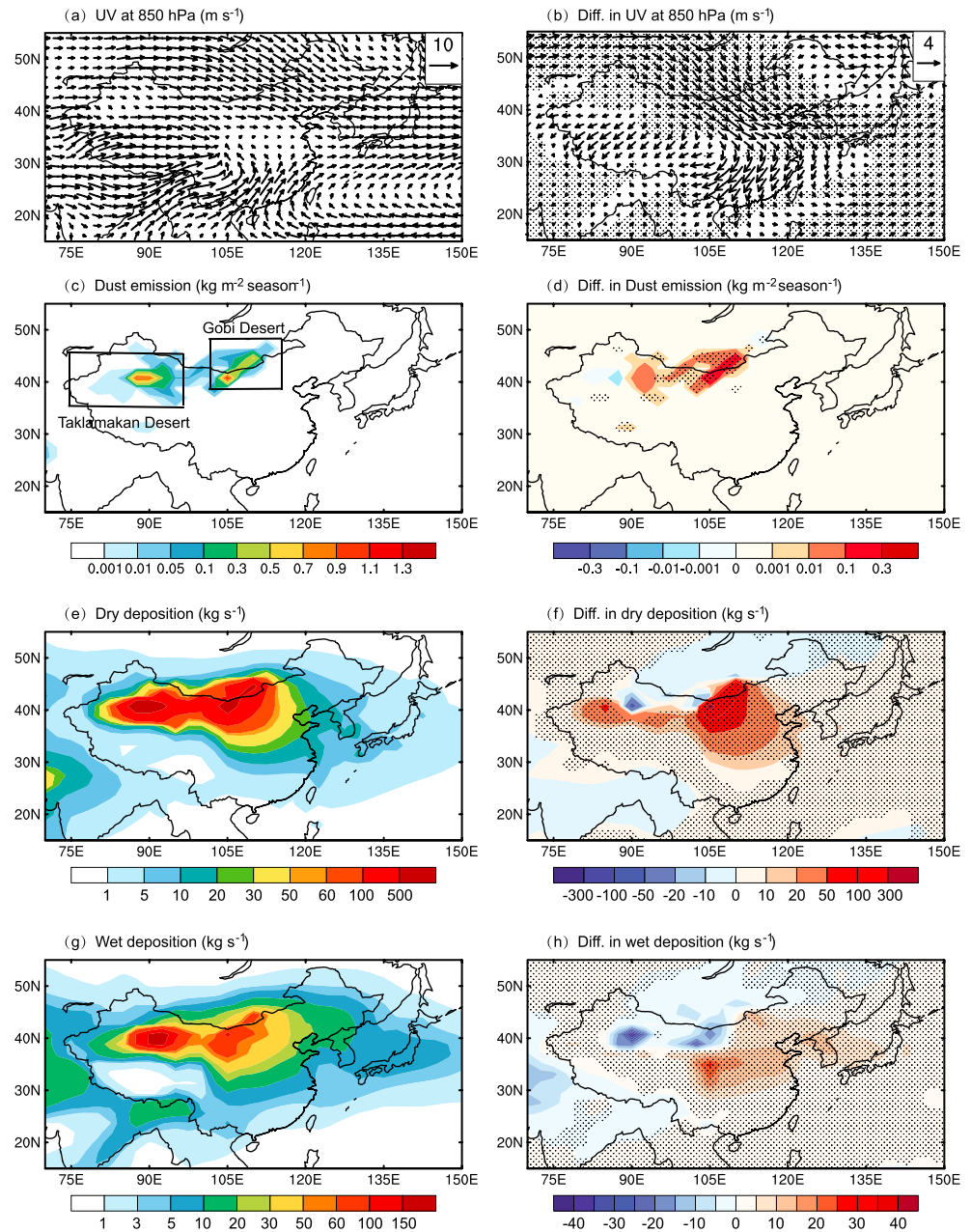


Figure 5. The MAM mean for (left column) 150 year simulation and (right column) differences between weakest and strongest EAM years (weakest-strongest) from IRUN in (a and b) horizontal winds at 850 hPa, (c and d) dust emissions, (e and f) dust dry deposition, and (g and h) dust wet deposition, respectively. The dotted areas indicate statistical significance with 95% (P value < 0.05) from a two-tailed Student's t test.

emissions in the PRUN simulation, we conclude that these differences are mainly due to the changes in transport and removal processes.

To understand the EAM impact on the dust mass budget, Table 1 shows the differences in dust burden, emission, and deposition between the weakest and strongest EAM years over China from the IRUN and PRUN simulations. Relative to the average dust burden, the difference between the weakest and the strongest EAM years over western China is 13.9% and 8.2% from the IRUN and PRUN, respectively. Considering the fixed dust emissions in the PRUN, the large increase in dust concentrations in the weakest EAM years is mainly due to the transport and deposition processes, which contribute 59% of the total difference (8.2% in PRUN relative to 13.9% in IRUN). Dust emission changes by only 4.9% in IRUN between the weakest and strongest

Table 1. Simulated MAM Dust Burden, Emissions, Deposition (Tg Season⁻¹), Lifetime (Days), Dry and Wet Removal Rates (day⁻¹) Over Eastern China (110°E–120°E, 20°N–45°N), Central China (100°E–110°E, 25°N–45°N), and Western China (75°E–100°E, 30°N–45°N) in the Weakest and Strongest EAM Years, as Well as the Absolute and Relative Difference

| | | IRUN | | | | PRUN | | | |
|---------------|-------------|--------|--------|--------|--------------------|-------|-------|--------|--------------------|
| | | Mean | Weak | Strong | Diff. ^a | Mean | Weak | Strong | Diff. ^a |
| Eastern China | Dust burden | 0.94 | 1.16 | 0.64 | 55.6% | 0.61 | 0.69 | 0.48 | 33.8% |
| | Emis. | 23.90 | 28.62 | 19.59 | 37.8% | - | - | - | - |
| | Dep. | 28.95 | 35.76 | 21.01 | 50.9% | 23.65 | 24.45 | 21.17 | 18.1% |
| | Life time | 2.99 | 2.98 | 2.67 | | 2.37 | 2.49 | 2.09 | |
| | Dry remov | 0.22 | 0.23 | 0.24 | | 0.31 | 0.29 | 0.34 | |
| | Wet remov | 0.11 | 0.10 | 0.14 | | 0.12 | 0.11 | 0.14 | |
| Central China | Dust burden | 0.96 | 1.07 | 0.79 | 29.6% | 0.77 | 0.79 | 0.71 | 10.3% |
| | Emis. | 87.69 | 103.72 | 70.90 | 37.4% | - | - | - | - |
| | Dep. | 44.40 | 50.52 | 37.97 | 28.2% | 54.07 | 53.73 | 53.68 | 0.1% |
| | Life time | 1.99 | 1.95 | 1.91 | | 1.31 | 1.35 | 1.22 | |
| | Dry remov | 0.39 | 0.41 | 0.39 | | 0.66 | 0.64 | 0.69 | |
| | Wet remov | 0.11 | 0.10 | 0.13 | | 0.10 | 0.10 | 0.13 | |
| Western China | Dust burden | 1.22 | 1.30 | 1.13 | 13.9% | 1.22 | 1.26 | 1.16 | 8.2% |
| | Emis. | 120.97 | 122.90 | 116.93 | 4.9% | - | - | - | - |
| | Dep. | 60.60 | 61.91 | 58.84 | 5.1% | 73.05 | 73.62 | 73.21 | 5.5% |
| | Life time | 1.85 | 1.93 | 1.77 | | 1.54 | 1.57 | 1.46 | |
| | Dry remov | 0.41 | 0.40 | 0.42 | | 0.56 | 0.55 | 0.57 | |
| | Wet remov | 0.13 | 0.12 | 0.15 | | 0.09 | 0.09 | 0.11 | |

^aAbsolute difference (Tg season⁻¹) and relative difference (100% × (weakest-strongest)/average).

EAM years because of the small variation in wind speed over the Taklamakan desert (TD) in western China (Figure 5b). Dry and wet deposition in IRUN increase over south of TD with increased dust concentrations in weak EAM years (Figures 5f and 5h) but decrease over north of TD because of the changes in emission region and less precipitation, respectively. The total dust deposition increases by 5.1% (IRUN) and 5.5% (PRUN) in the weakest EAM years than those in the strongest EAM years, respectively. We also follow *Textor et al.* [2006] to calculate the regional residence time for dust by $\tau = \frac{\text{burden}}{\text{sinks}}$ and the effective removal rate coefficients for dry and wet deposition by $k_i = \sum \frac{\text{massflux}_{\text{sink}i}}{(\text{massflux}_{\text{sink}i})} \times \frac{1}{\tau}$, where i is the number of sinks

considered and $\text{massflux}_{\text{sink}i}$ represents the regional mass flux of individual sink i . Over western China, the residence time for dust is about 2 days in IRUN, which is shorter than the global model average of about 4 days, but falls within the range of 16 AeroCom models given in *Textor et al.* [2006]. The simulated shorter lifetime of dust is because of the large magnitude of dry deposition near the source region, with a larger dry removal rate coefficient of 0.41 day⁻¹ in IRUN compared to that of 0.23 day⁻¹ in *Textor et al.* [2006]. The effective removal rates for both dry and wet scavenging in IRUN are always lower in the weakest EAM years than those in the strongest years, partially due to the smaller wet deposition (Figure 5h). The lower removal rates indicate a longer lifetime of dust during the weakest EAM years in western China.

In central China, the difference in dust burden between the weakest and strongest EAM years is found to be 29.6% in IRUN. The difference in dust concentration is mainly due to the variations in dust emissions by up to 37.4% relative to the regional mean value. The transport and deposition processes lead to a 10.3% difference between the weakest and strongest EAM years. The effective removal rates for wet scavenging are also lower in weak EAM years compared to strong EAM years, with values of 0.10 and 0.13 day⁻¹, respectively. However, the effective removal rate for dry deposition is higher in weak EAM years, because of large gravitational settling near the dust source region (Figure 5f). It should be noted that the difference in total deposition processes between the weakest and strongest EAM years is only 0.1% in the PRUN, suggesting that the deposition does not play an important role in central China.

The difference in dust burden between the weakest and strongest EAM years over eastern China is found to be 55.6% in the IRUN relative to the regional mean value, with a 33.8% contribution from the stronger transport of dust associated with strong northwesterly winds (Figure 5b) and deposition processes in the PRUN, which contributes 60.7% of the total difference. Relative to the mean value, the change in dust emissions

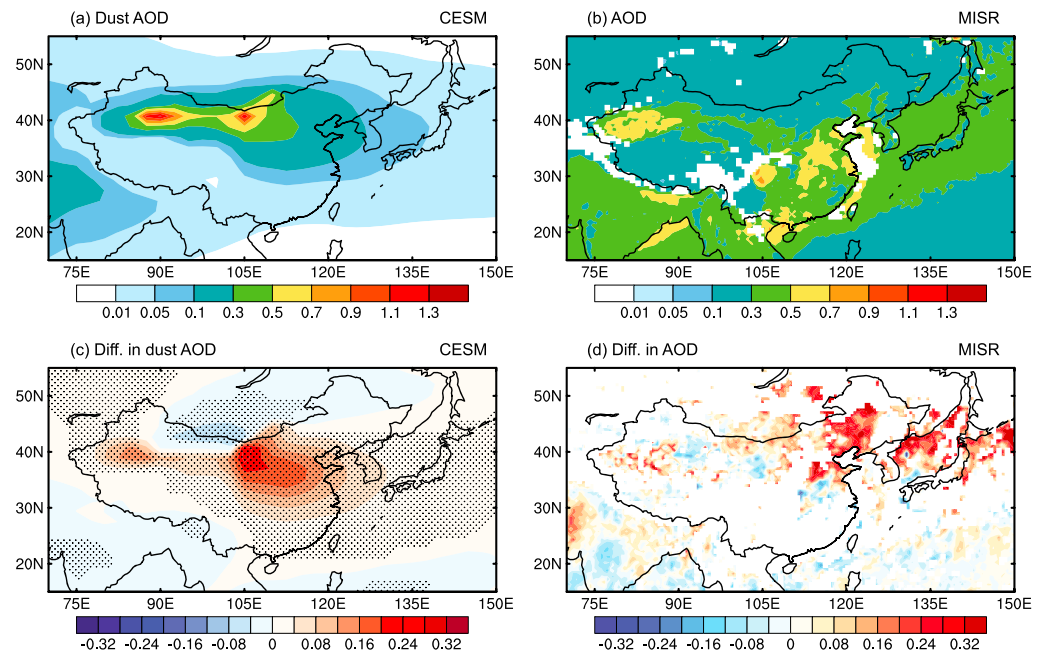


Figure 6. Comparisons of (left column) simulated dust optical depth (AOD) with (right column) the MISR AOD. The top plot averaged MAM AOD for (a) 150 year simulation and (b) years 2000–2014. The bottom plot shows (c) the differences in AOD between the weakest and strongest EAM years (weakest-strongest), and (d) the differences between year 2011 (weakest) and 2003 (strongest). The dotted areas indicate statistical significance with 95% (P value < 0.05) from a two-tailed Student’s t test. The simulated AOD are from IRUN.

in IRUN over eastern China between the weakest and strongest EAM years is 37.8%, highlighting the contribution from the variations in wind speed. Over eastern China, the residence time for dust is about 3 days in IRUN; the simulated shorter lifetime of dust is because of the large magnitude of wet scavenging downwind of high source regions, with a larger wet removal rate coefficient of 0.11 day^{-1} in IRUN compared to that of 0.08 day^{-1} in *Textor et al.* [2006]. The effective removal rates in IRUN for both dry and wet scavenging are also lower in the weakest EAM years over eastern China, with values of 0.23 and 0.10 day^{-1} , relative to the values of 0.24 and 0.14 day^{-1} , respectively, in the strongest EAM years.

4. Discussion

Figure 6a shows the simulated mean MAM dust aerosol optical depth (AOD) in the IRUN simulation. The simulated mean dust AOD values are in the range of 0.05–0.3 over a large fraction of China, with maximum values of up to 1.1 over the Gobi and Taklamakan deserts. The mean MAM distributions of AODs retrieved from the Multiangle Imaging Spectroradiometer (MISR) during 2000–2012 are shown in Figure 6b, with larger AODs in the range of 0.3–0.7 over eastern China than those in the IRUN as a result of the high concentrations of anthropogenic aerosols in this region [X. Y. Zhang et al., 2012; Lou et al., 2014], which we did not include in the simulation. Although the MISR also captures the pattern of large AOD values over western and central north China, the AOD values are much smaller around dust source regions, with values in the range of 0.3–0.7. The high biases of simulated AOD in dust source regions can be explained by the overestimation of dust aerosol burdens in that region because of the large changes in dust source area associated with vegetation, precipitation, temperature, and cloudiness due to the anthropogenic activities [Mahowald et al., 2006a, 2006b; Gu et al., 2010; Jiang et al., 2015], as well as a higher relative humidity over the Gobi desert in the preindustrial scenario (Figure S5) relative to the current days.

The impacts of variations in wind field on dust AOD are evaluated by examining the difference in AOD between the weakest and strongest EAM years (weakest-strongest) (Figure 6c). Relative to the strongest EAM years, the AOD is higher by up to 0.20, 0.28, and 0.16 over eastern, central, and western China in the weakest EAM years, respectively, which is in agreement with the largest increment in dust aerosol concentrations (Figure 3a). The differences in MISR AOD values between year 2011 and 2003 (weakest and strongest

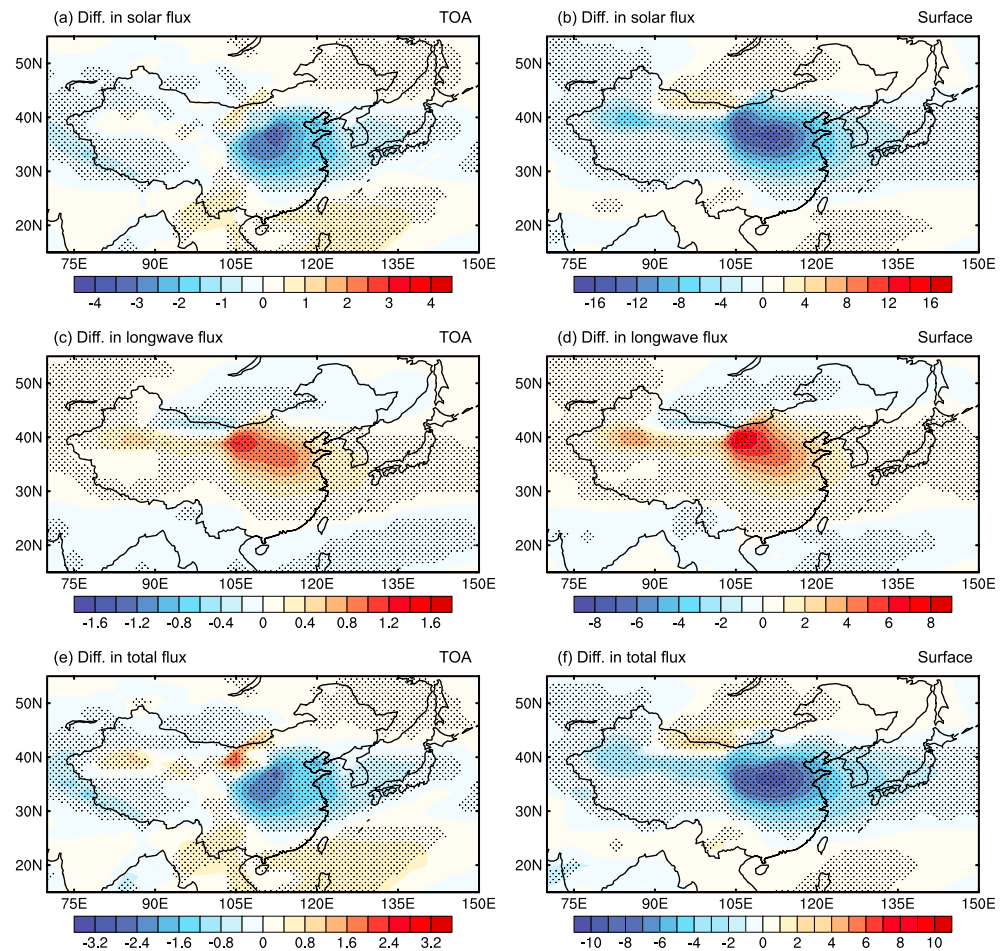


Figure 7. The direct radiative forcing differences in (a and b) solar flux, (c and d) long-wave flux, and (e and f) total flux by dust between the weakest and strongest EAM years (weakest-strongest) in the IRUN. Left column shows changes at the top of the atmosphere, and right column shows changes at the surface. The dotted areas indicate statistical significance with 95% (P value < 0.05) from a two-tailed Student's t test. Positive (negative) value refers to net downward (upward) flux.

EAM year) show even larger increases in AOD of up to 0.3 over eastern China (Figure 6d), partially due to the increase in anthropogenic emissions in recent decades [Q. Zhang *et al.*, 2012]. Without impacts from anthropogenic aerosols, the differences in MISR AOD values over western China have a similar pattern to simulated AOD, indicating increased dust concentrations in weak EAM years.

To determine the radiative forcing by the changes in the dust distributions, we have calculated the EAM dust direct radiative forcing as the difference in the direct radiative forcing of all aerosol between weak and strong EAM years. The direct radiative forcing of all aerosol is diagnosed from the difference between the radiative flux calculated with all aerosol and with no aerosol, for the same clouds, water vapor, and temperature distributions [Ghan, 2013]. Figure 7 shows the EAM dust direct radiative forcing for the solar flux, long-wave flux, and net flux at the top of the atmosphere (TOA; Figure 7, left column) and at the surface (Figure 7, right column) in the IRUN. Over eastern China, the differences in short-wave radiative forcing (SWRF) at both the TOA and surface are mostly negative, with values of up to -3.5 W m^{-2} (TOA) and -14 W m^{-2} (surface) in the area downwind of source regions, resulting from the increased AOD (dust concentrations) of up to 0.2 (210 mg m^{-2}), due to the dominant contribution of reflection in the short-wave spectrum [Shell and Somerville, 2007]. Our results are consistent with the changes in total dust radiative forcing with dust AOD or dust concentrations of Zhang *et al.* [2009] and Park *et al.* [2010]. Zhang *et al.* [2009] found that the dust aerosol SWRF at the TOA and at the surface are in the range of -2.5 to -5 W m^{-2} and -5 to -10 W m^{-2} , respectively, with dust AOD values of 0.1–0.2 over eastern China during February–March–April–May, based on a 10 year simulation with the Regional Climate Model RegCM version 3 model. Park *et al.* [2010] reported

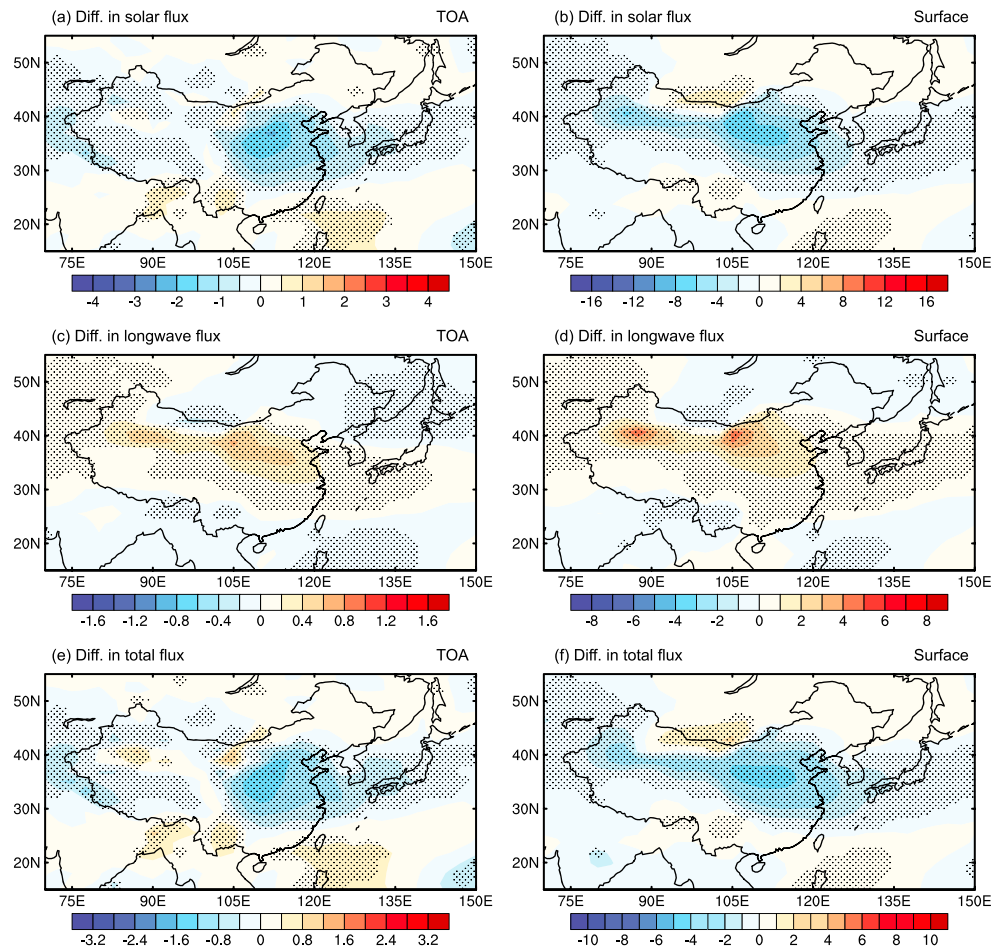


Figure 8. The same as Figure 7 but in the prescribed emission run (PRUN).

the SW forcing at the surface between -10 and -20 W m^{-2} over eastern China due to dust column concentrations in the range of $200\text{--}1000 \text{ mg m}^{-2}$ on 19 March 2002, using the MM5 model and the Asian Dust Aerosol Model. It should be noted that the differences in SWRF between the weakest and strongest EAM years over western China are still negative at the surface due to the scattering and absorption of sunlight by mineral dust, but positive at the TOA over the Taklamakan desert because of the relatively high albedo (Figures 7a and 7b), with maximum values of -8 and $+1 \text{ W m}^{-2}$, in agreement with previous studies [Liao and Seinfeld, 1998; Yue *et al.*, 2010]. The differences in SWRF at the TOA and surface by dust aerosol in the PRUN between the weakest and strongest EAM years show a similar pattern (Figures 8a and 8b), with values of up to -2 W m^{-2} (TOA) and -8 W m^{-2} (surface) in the area downwind of source regions, smaller than those in the IRUN. These results indicate that the interannual variations in dust emissions enhance the impact of EAM on SWRF over eastern China by about 43%. Excluding the effects of the differences in dust size distributions between IRUN and PRUN would make the impact of EAM on SWRF even larger.

Relative to the strongest EAM years, the long-wave radiative forcing (LWRF) is larger in the weakest EAM years over a large fraction of China in the IRUN (Figures 7c and 7d) because of the large increase in dust column burden (Figure 3a), with the largest LWRF values of $+1.2$ and $+7 \text{ W m}^{-2}$ over the Gobi desert at the TOA and at the surface, respectively. Over western China, the LWRF increases by $+0.6$ and $+4 \text{ W m}^{-2}$ over the Taklamakan desert resulting from the increment of dust AOD by up to 0.16. The increased LWRF between the weakest and strongest EAM years is found to be even larger with prescribed dust emissions over western China (Figures 8c and 8d) than that in the IRUN, suggesting that the interannual variations in dust emissions offset the impact of EAM on LWRF over western China because of the changes in dust source regions (Figure 5d).

The results from the differences in net RF between the weakest and strongest EAM years indicate cooling at the surface in the weakest EAM years. At the TOA, there is still cooling over eastern China, but warming over the dust source region in central and western China in the weakest EAM years compared to the strongest EAM years. The cooling due to the net RF is in the range of -0.4 to -2.4 W m^{-2} at the TOA and of -1 to -9 W m^{-2} at the surface, while the warming is in the range of $+0.4$ to $+1.2 \text{ W m}^{-2}$ and $+0.8$ to $+2.4 \text{ W m}^{-2}$ at the TOA over the Taklamakan and Gobi deserts, respectively. This pattern in net RF agrees with that found by *Liao et al.* [2004] and *Zhang et al.* [2009]. Compared to the PRUN (Figures 8e and 8f), the interannual variations in dust emissions significantly enhance the impact of EAM on net RF over eastern China both at the TOA and surface by about 40%, but slightly offset the influence over western China.

It should be noted that the OPAC overestimates the dust absorption at both shortwave and longwave spectral ranges compared to measurements of Saharan mineral dust and over the Mediterranean [*Di Biagio et al.*, 2014; *Denjean et al.*, 2016]. Since dust absorption is overestimated, the direct radiative forcing induced by dust aerosol over eastern China simulated by the model is larger at the surface but smaller at the TOA than it should be. Moreover, anthropogenic aerosols have been shown to increase surface temperature, precipitation over northwestern China, and also weaken the northwesterly winds from Gobi desert to eastern China in spring [*Gu et al.*, 2010; *Jiang et al.*, 2015], all of which would reduce both dust emissions and the transported mass flux of dust. Therefore, the change in direct radiative forcing due to changes in dust is reduced when anthropogenic aerosols are also included in the model.

5. Conclusions

We consider the wind variation as an annual cycle and examine the impacts of the East Asian Monsoon (EAM) on interannual variations of springtime dust concentrations over China using the Community Earth System Model (CESM). The interannual variations of dust concentrations are quantified by values of standard deviation (SD) and relative standard deviation (RSD) based on 150 year simulations. The SD values of dust column burden are in the range of 20 – 200 mg m^{-2} over a large fraction of China, with the largest values exceeding 300 mg m^{-2} around the Gobi and Taklamakan deserts. The RSD values of MAM dust concentrations are 20–40% in northeastern China, 10–20% in northwestern China, 30–50% in southeastern China, and 50–70% over the Tibetan Plateau.

Both simulated MAM dust concentrations and Total Ozone Mapping Spectrometer Aerosol Index (TOMS AI) show a strong negative correlation with the East Asian Monsoon Index (EAMI) over a large fraction of China, with regional averaged correlation coefficients of -0.64 and -0.25 over eastern China (105 – 120°E , 25 – 40°N), respectively, indicating that the changes in dust burden result from the interannual variations of the wind field. The MAM dust concentrations are higher (or lower) in weaker (or stronger) EAM years over almost all of China. The regional mean dust burden in the weakest EAM years is higher than those in the strongest EAM years by 55.6%, 29.6%, and 13.9% in the interactive simulation in eastern, central, and western China, respectively, and by 33.8%, 10.3%, and 8.2% with prescribed dust emissions in PRUN simulation. These results indicate that the transport and deposition processes contribute about 60% of the total difference in dust burden, while the variation in dust emissions contributes about 40%. The anomalously high northwesterly winds through the Gobi desert and westerly winds through the Taklamakan desert lead to significant changes in both dust emissions and transport flux, which cause variations in dust concentrations in China.

Both simulated dust AOD and those from the Multiangle Imaging Spectroradiometer (MISR) show larger AOD values in weak EAM years than in strong EAM years over a large fraction of China. The increase in AOD by up to 0.2 changes shortwave radiative forcing (SWRF) by up to -16 and -8 W m^{-2} at the surface and -4 and $+1 \text{ W m}^{-2}$ at the TOA over eastern and western China, respectively. Simulated differences in longwave radiative forcing (LWRF) between the weakest and strongest EAM years are $+6$ and $+4 \text{ W m}^{-2}$ at the surface and $+1$ and $+0.6 \text{ W m}^{-2}$ at the TOA over eastern and western China, respectively. The net RF is always negative in eastern China, with maximum values of -9 and -2.4 W m^{-2} at the surface and TOA, respectively, and is positive in western China at TOA, by up to $+1.2 \text{ W m}^{-2}$. The interannual variations in dust emissions enhance the impact of EAM on SWRF by about 43% over eastern China but offset the impact of EAM on LWRF over western China. Therefore, the impact of EAM on net RF over eastern China is enhanced by about 40% but is slightly offset over western China due to the interactive dust emissions.

Acknowledgments

This research was supported by National Science Foundation AGS1048995 and by DOE DE-SC0006679 as part of the U.S. Department of Energy, Office of Science, Biological, and Environmental Research, Decadal and Regional Climate Prediction using Earth System Models program. The Pacific Northwest National Laboratory is operated for the DOE by Battelle Memorial Institute under contract DE-AC05-76RLO 1830. NCEP Reanalysis data sets are provided by the NOAA/OAR/ESRL PSD, Boulder, Colorado, USA, from their Web site at <http://www.esrl.noaa.gov/psd/>. The satellite-derived Total Ozone Mapping Spectrometer Aerosol Index (TOMS AI) monthly data sets are obtained from the Web site at <http://www.ouce.ox.ac.uk/~clivar/tomsai/aiinput.html>. Multiangle Imaging Spectroradiometer (MISR) data sets are provided by NASA's Jet Propulsion Laboratory, Pasadena, California, from their Web site at <https://eosweb.larc.nasa.gov/project/misr/>. This research used resources of the National Energy Research Scientific Computing Center under contract DE-AC02-05CH11231. The data and codes for these results are posted at http://portal.nersc.gov/project/m1374/EAM_DUST.

References

- Abulaiti, A., R. Kimura, M. Shinoda, Y. Kurosaki, M. Mikami, M. Ishizuka, Y. Yamada, E. Nishihara, and B. Gantsetseg (2014), An observational study of saltation and dust emission in a hotspot of Mongolia, *Aeolian Res.*, *15*, 169–176.
- Ackerman, S. A., and H. Chung (1992), Radiative effects of airborne dust on regional energy budgets at the top of the atmosphere, *J. Appl. Meteorol.*, *31*(2), 223–233, doi:10.1175/1520-0450(1992)031<0223:REOADO>2.0.CO;2.
- Ahn, H.-J., S.-U. Park, and L.-S. Chang (2007), Effect of direct radiative forcing of Asian dust on the meteorological fields in East Asia during an Asian dust event period, *J. Appl. Meteorol. Climatol.*, *46*, 1655–1681.
- Bangalath, H. K., and G. Stenichkov (2015), Role of dust direct radiative effect on the tropical rain belt over Middle East and North Africa: A high-resolution AGCM study, *J. Geophys. Res. Atmos.*, *120*, 4564–4584, doi:10.1002/2015JD023122.
- Carlson, T. N., and S. G. Benjamin (1980), Radiative heating rates for Saharan dust, *J. Atmos. Sci.*, *37*, 193–213.
- Cautenet, G., M. Legrand, S. Cautenet, B. Bonnel, and G. Brogniez (1991), Thermal impact of Saharan dust over land. Part I: Simulation, *J. Appl. Meteorol.*, *31*, 166–180, doi:10.1175/1520-0450(1992)031<0166:TIOSDO>2.0.CO;2.
- Chen, W., D. W. Fryrear, and Z. Yang (1999), Dust fall in the Taklamakan desert of China, *Phys. Geogr.*, *20*, 189–224.
- DeFlorio, M. J., I. D. Goodwin, D. R. Cayan, A. J. Miller, S. J. Ghan, D. W. Pierce, L. M. Russell, and B. Singh (2015), Interannual modulation of subtropical Atlantic boreal summer dust variability by ENSO, *Clim. Dyn.*, doi:10.1007/s00382-015-2600-7.
- Denjean, C., et al. (2016), Size distribution and optical properties of mineral dust aerosols transported in the western Mediterranean, *Atmos. Chem. Phys.*, *16*, 1081–1104, doi:10.5194/acp-16-1081-2016.
- Di Biagio, C. D., H. Boucher, S. Caqueneau, S. Chevaillier, J. Cuesta, and P. Formenti (2014), Variability of the infrared complex refractive index of African mineral dust: Experimental estimation and implications for radiative transfer and satellite remote sensing, *Atmos. Chem. Phys.*, *14*, 11,093–11,116, doi:10.5194/acp-14-11093-2014.
- Doherty, O. M., N. Riemer, and Z. Yang (1999), Control of Saharan mineral dust transport to Barbados in winter by the Intertropical Convergence Zone over West Africa, *Tellus B.*, doi:10.3402/tellusb.v66.23191.
- Duce, R. A., C. K. Unni, B. J. Ray, J. M. Prospero, and J. T. Merrill (1980), Long-range atmospheric transport of soil dust from Asia to the tropical North Pacific: Temporal variability, *Science*, *209*, 1522–1524.
- Ghan, S. J. (2013), Technical note: Estimating aerosol effects on cloud radiative forcing, *Atmos. Chem. Phys.*, *13*, 9971–9974, doi:10.5194/acp-13-9971-2013.
- Ghan, S. J., and R. A. Zaveri (2007), Parameterization of optical properties for hydrated internally mixed aerosol, *J. Geophys. Res.*, *112*, D10201, doi:10.1029/2006JD007927.
- Gong, S. L., X. Y. Zhang, T. L. Zhao, I. G. McKendry, D. A. Jaffe, and N. M. Lu (2003), Characterization of soil dust aerosol in China and its transport and distribution during 2001 ACE-Asia: 2. Model simulation and validation, *J. Geophys. Res.*, *108*(D9), 4262, doi:10.1029/2002JD002633.
- Gong, S. L., X. Y. Zhang, T. L. Zhao, X. B. Zhang, L. A. Barrie, I. G. McKendry, and C. S. Zhao (2006), A simulated climatology of Asian dust aerosol and its trans-Pacific transport. Part II: Interannual variability and climate connections, *J. Clim.*, *19*, 104–122, doi:10.1175/JCLI3606.1.
- Gu, Y., K. N. Liou, W. Chen, and H. Liao (2010), Direct climate effect of black carbon in China and its impact on dust storms, *J. Geophys. Res.*, *115*, D00K14, doi:10.1029/2009JD013427.
- Guo, H., M. Xu, and Q. Hu (2011), Changes in near-surface wind speed in China: 1969–2005, *Int. J. Climatol.*, *31*, 349–358, doi:10.1002/joc.2091.
- Hara, Y., I. Uno, and Z. Wang (2006), Long-term variation of Asian dust and related climate factors, *Atmos. Environ.*, *40*, 6730–6740.
- Haywood, J. M., R. P. Allan, I. Culverwell, T. Slingo, S. Milton, J. Edwards, and N. Clerbaux (2005), Can desert dust explain the outgoing longwave radiation anomaly over the Sahara during July 2003? *J. Geophys. Res.*, *110*, D05105, doi:10.1029/2004JD005232.
- He, Y. J., I. Uno, Z. F. Wang, P. Pochanart, J. Li, and H. Akimoto (2008), Significant impact of the East Asian Monsoon on ozone seasonal behavior in the boundary layer of Eastern China and the west Pacific region, *Atmos. Chem. Phys.*, *8*, 7543–7555, doi:10.5194/acp-8-7543-2008.
- Hess, M., P. Koepke, and I. Schult (1998), Optical properties of aerosols and clouds: The software package OPAC, *Bull. Am. Meteorol. Soc.*, *79*(5), 831–844.
- Holzer, M., I. G. McKendry, and D. A. Jaffe (2003), Springtime trans-Pacific atmospheric transport from east Asia: A transit-time probability density function approach, *J. Geophys. Res.*, *108*(D22), 4708, doi:10.1029/2003JD003558.
- Hurrell, J. W., et al. (2013), The Community Earth System Model: A framework for collaborative research, *Bull. Am. Meteorol. Soc.*, *94*, 1339–1360, doi:10.1175/BAMS-D-12-00121.1.
- Husar, R. B., J. M. Prospero, and L. L. Stowe (1997), Characterization of tropospheric aerosols over the oceans with the NOAA advanced very high resolution radiometer optical thickness operational product, *J. Geophys. Res.*, *102*, 16,889–16,909, doi:10.1029/96JD04009.
- Husar, R. B., et al. (2001), Asian dust event of April 1998, *J. Geophys. Res.*, *106*, 18,317–18,330, doi:10.1029/2000JD900788.
- Intergovernmental Panel on Climate Change (2013), Climate change 2013: The physical science basis, in *Contribution of Working Group I to the Fifth Assessment Report of the Intergovernmental Panel on Climate Change*, edited by T. F. Stocker et al., pp. 1–1535, Cambridge Univ. Press, Cambridge, U. K., and New York.
- Jiang, Y., X. Yang, and X. Liu (2015), Seasonality in anthropogenic aerosol effects on East Asian climate simulated with CAM5, *J. Geophys. Res. Atmos.*, *120*, 10,837–10,861, doi:10.1002/2015JD023451.
- Jin, Q., J. Wei, and Z.-L. Yang (2014), Positive response of Indian summer rainfall to Middle East dust, *Geophys. Res. Lett.*, *41*, 4068–4074, doi:10.1002/2014GL059980.
- Kimura, R. (2012), Effect of strong wind and land cover in dust source regions on the Asian dust event over Japan from 2000 to 2011, *SOLA*, *8*, 77–80, doi:10.2151/sola.2012-020.
- Lee, J.-J., and C.-H. Kim (2012), Roles of surface wind, NDVI and snow cover in the recent changes in Asian dust storm occurrence frequency, *Atmos. Environ.*, *59*, 366–375, doi:10.1016/j.atmosenv.2012.05.022.
- Li, J., and Q. Zeng (2002), A unified monsoon index, *Geophys. Res. Lett.*, *29*(8), 1274, doi:10.1029/2001GL013874.
- Li, X., and H. Zhang (2012), Seasonal variations in dust concentration and dust emission observed over Horqin Sandy Land area in China from December 2010 to November 2011, *Atmos. Environ.*, *61*, 56–65, doi:10.1016/j.atmosenv.2012.07.007.
- Liao, H., and J. H. Seinfeld (1998), Radiative forcing by mineral dust aerosols: Sensitivity to key variables, *J. Geophys. Res.*, *103*, 31,637–31,645, doi:10.1029/1998JD200036.
- Liao, H., J. H. Seinfeld, P. J. Adams, and L. J. Mickley (2004), Global radiative forcing of coupled tropospheric ozone and aerosols in a unified general circulation model, *J. Geophys. Res.*, *109*, D16207, doi:10.1029/2003JD004456.
- Liu, X., Z.-Y. Yin, X. Zhang, and X. Yang (2004), Analyses of the spring dust storm frequency of northern China in relation to antecedent and concurrent wind, precipitation, vegetation, and soil moisture conditions, *J. Geophys. Res.*, *109*, D16210, doi:10.1029/2004JD004615.
- Liu, X., et al. (2012), Toward a minimal representation of aerosols in climate models: Description and evaluation in the Community Atmosphere Model CAM5, *Geosci. Model Dev.*, *5*, 709–739, doi:10.5194/gmd-5-709-2012.

- Lou, S., H. Liao, and B. Zhu (2014), Impacts of aerosols on surface-layer ozone concentrations in China through heterogeneous reactions and changes in photolysis rates, *Atmos. Environ.*, *85*, 123–138, doi:10.1016/j.atmosenv.2013.12.004.
- Mahowald, N., D. R. Muhs, S. Levis, P. J. Rasch, M. Yoshioka, C. S. Zender, and C. Luo (2006a), Change in atmospheric mineral aerosols in response to climate: Last glacial period, preindustrial, modern, and doubled carbon dioxide climates, *J. Geophys. Res.*, *111*, D10202, doi:10.1029/2005JD006653.
- Mahowald, N., M. Yoshioka, W. Collins, A. Conley, D. Fillmore, and D. Coleman (2006b), Climate response and radiative forcing from mineral aerosols during the last glacial maximum, pre-industrial and doubled-carbon dioxide climates, *Geophys. Res. Lett.*, *33*, L20705, doi:10.1029/2006GL026126.
- Markowicz, K. M., P. J. Flatau, A. M. Vogelmann, P. K. Quinn, and E. J. Welton (2003), Clear-sky infrared aerosol radiative forcing at the surface and the top of the atmosphere, *Q. J. R. Meteorol. Soc.*, *129*(594), 2927–2947, doi:10.1256/qj.02.224.
- Merrill, J. T., M. Uematsu, and R. Bleck (1989), Meteorological analysis of long range transport of mineral aerosols over the North Pacific, *J. Geophys. Res.*, *94*, 8584–8598, doi:10.1029/JD094iD06p08584.
- Miller, R. L., and I. Tegen (1998), Climate response to soil dust aerosols, *J. Clim.*, *11*(12), 3247–3267, doi:10.1175/1520-0442(1998)011<3247:CRTSDA>2.0.CO;2.
- Park, S.-U., H.-J. Ahn, and M.-S. Park (2010), Direct shortwave radiative forcing of the Asian dust aerosol on dust emission, *Theor. Appl. Climatol.*, *101*, 179–190, doi:10.1007/s00704-009-0245-3.
- Prijith, S. S., M. Aloysius, and M. Mohan (2013), Global aerosol source/sink map, *Atmos. Environ.*, *80*, 533–539, doi:10.1016/j.atmosenv.2013.08.038.
- Qian, W., X. Tang, and L. Quan (2004), Regional characteristics of dust storms in China, *Atmos. Environ.*, *38*, 4895–4907, doi:10.1016/j.atmosenv.2004.05.038.
- Satheesh, S. K., C. B. S. Dutt, J. Srinivasan, and U. R. Rao (2007), Atmospheric warming due to the dust absorption over Afro-Asian regions, *Geophys. Res. Lett.*, *34*, L04805, doi:10.1029/2006GL028623.
- Shell, K. M., and R. C. J. Somerville (2007), Direct radiative effect of mineral dust and volcanic aerosols in a simple aerosol climate model, *J. Geophys. Res.*, *112*, D03206, doi:10.1029/2006JD007198.
- Small, R. J., et al. (2014), A new synoptic scale resolving global climate simulation using the Community Earth System Model, *J. Adv. Mod. Earth Systems*, *6*, 1065–1094, doi:10.1002/2014MS000363.
- Smith R., et al. (2010), The Parallel Ocean Program (POP) reference manual, Tech. Rep. LAUR-10-01853, Los Alamos Natl. Lab.
- Sokolik, I. N., and O. B. Toon (1996), Direct radiative forcing by anthropogenic airborne mineral aerosols, *Nature*, *381*, 681–683, doi:10.1038/381681a0.
- Sun, J., M. Zhang, and T. Liu (2001), Spatial and temporal characteristics of dust storms in China and its surrounding regions, 1960–1999: Relations to source area and climate, *J. Geophys. Res.*, *106*, 10,325–10,333, doi:10.1029/2000JD900665.
- Tan, S.-C., G.-Y. Shi, and H. Wang (2012), Long-range transport of spring dust storms in Inner Mongolia and impact on the China seas, *Atmos. Environ.*, *46*, 299–308, doi:10.1016/j.atmosenv.2011.09.058.
- Tanaka, T. Y., T. T. Sekiyama, T. Maki, and M. Mikami (2011), The effects of snow cover and soil moisture on Asian dust: I. A numerical sensitivity study, *SOAL*, *7A*, 36–39, doi:10.2151/sola.7A-010.
- Textor, C., et al. (2006), Analysis and quantification of the diversities of aerosol life cycles within AeroCom, *Atmos. Chem. Phys.*, *6*, 1777–1813, doi:10.5194/acp-6-1777-2006.
- Uematsu, M., R. A. Duce, J. M. Prospero, L. Chen, J. T. Merrill, and R. L. McDonald (1983), Transport of mineral aerosol from Asia over the North Pacific Ocean, *J. Geophys. Res.*, *88*, 5343–5352, doi:10.1029/JC088iC09p05343.
- Uno, I., et al. (2003), Regional chemical weather forecasting system CFORS: Model descriptions and analysis of surface observations at Japanese island stations during the ACE-Asia experiment, *J. Geophys. Res.*, *108*, 8668, doi:10.1029/2002JD002845.
- Wang, C. (2013), Impact of anthropogenic absorbing aerosols on clouds and precipitation: A review of recent progresses, *Atmos. Res.*, *122*(D23), 237–249, doi:10.1016/j.atmosres.2012.11.005.
- Wang, Y. Q., X. Y. Zhang, R. Arimoto, J. J. Cao, and Z. X. Shen (2004), The transport pathways and sources of PM10 pollution in Beijing during spring 2001, 2002 and 2003, *Geophys. Res. Lett.*, *31*, L14110, doi:10.1029/2004GL019732.
- Wang, Y. Q., X. Y. Zhang, S. L. Gong, C. H. Zhou, X. Q. Hu, H. L. Liu, T. Niu, and Y. Q. Yang (2008), Surface observation of sand and dust storm in East Asia and its application in CUACE/Dust, *Atmos. Chem. Phys.*, *8*, 545–553, doi:10.5194/acp-8-545-2008.
- Wang, Z., Y. Li, B. Liu, and J. Liu (2015), Global climate internal variability in a 2000-year control simulation with Community Earth System Model (CESM), *Chinese Geogr. Sci.*, *25*, 263–273, doi:10.1007/s11769-015-0754-1.
- Webster, P. J., and S. Yang (1992), Monsoon and ENSO: Selectively interactive systems, *Q. J. R. Meteorol. Soc.*, *118*, 877–926.
- Xuan, J., and I. N. Sokolik (2002), Characterization of sources and emission rates of mineral dust in Northern China, *Atmos. Environ.*, *36*, 4863–4876, doi:10.1016/S1352-2310(02)00585-X.
- Yang, Y., H. Liao, and J. Li (2014), Impacts of the East Asian summer monsoon on interannual variations of summertime surface-layer ozone concentrations over China, *Atmos. Chem. Phys.*, *14*, 6867–6879, doi:10.5194/acp-14-6867-2014.
- Yang, Y., H. Liao, and S. Lou (2015), Decadal trend and interannual variation of outflow of aerosols from East Asia: Roles of variations in meteorological parameters and emissions, *Atmos. Environ.*, *100*, 141–153, doi:10.1016/j.atmosenv.2014.11.004.
- Yang, Y., et al. (2016a), Impacts of ENSO events on cloud radiative effects in preindustrial conditions: Changes in cloud fraction and their dependence on interactive aerosol emissions and concentrations, *J. Geophys. Res. Atmos.*, *121*, 6321–6335, doi:10.1002/2015JD024503.
- Yang, Y., L. M. Russell, S. Lou, Y. Liu, B. Singh, and S. J. Ghan (2016b), Rain-aerosol relationships influenced by wind speed, *Geophys. Res. Lett.*, *43*, 2267–2274, doi:10.1002/2016GL067770.
- Yue, X., H. Wang, H. Liao, and K. Fan (2010), Simulation of dust aerosol radiative feedback using the GMOD: 2. Dust-climate interactions, *J. Geophys. Res.*, *115*, D04201, doi:10.1029/2009JD012063.
- Yumimoto, K., and T. Takemura (2015), Long-term inverse modeling of Asian dust: Interannual variations of its emission, transport, deposition, and radiative forcing, *J. Geophys. Res. Atmos.*, *120*, 1582–1607, doi:10.1002/2014JD022390.
- Zender, C. S., H. Bian, and D. L. Newman (2003), The mineral dust entrainment and deposition (DEAD) model: Description and 1990s dust climatology, *J. Geophys. Res.*, *108*(D14), 4416, doi:10.1029/2002JD002775.
- Zhang, D. F., A. S. Zakey, X. J. Gao, F. Giorgi, and F. Solmon (2009), Simulation of dust aerosol and its regional feedbacks over East Asia using a regional climate model, *Atmos. Chem. Phys.*, *9*, 1095–1110, doi:10.5194/acp-9-1095-2009.
- Zhang, Q., G. Geng, S. Wang, A. Richter, and K. He (2012), Satellite remote sensing of changes in NO_x emissions over China during 1996–2010, *Chinese Sci. Bull.*, *57*, 2857–2864, doi:10.1007/s11434-012-5015-4.
- Zhang, T.-H., and H. Liao (2016), Aerosol absorption optical depth of fine-mode mineral dust in eastern China, *Atmos. Ocea. Sci. Lett.*, *9*(1), 7–14.

- Zhang, X., Z. Shen, G. Zhang, T. Chen, and H. Liu (1996), Remote mineral aerosol in westerlies and their contributions to Chinese loess, *Sci. China*, *39D*, 67–76.
- Zhang, X., R. Arimoto, and Z. S. An (1997), Dust emission from Chinese desert sources linked to variations in atmospheric circulation, *J. Geophys. Res.*, *102*, 28,041–28,047, doi:10.1029/97JD02300.
- Zhang, X., R. Arimoto, G. H. Zhu, T. Chen, and G. Y. Zhang (1998), Concentration, size-distribution and deposition of mineral aerosol over Chinese desert regions, *Tellus B*, *50*, 317–330, doi:10.1034/j.1600-0889.1998.t01-3-0001.x.
- Zhang, X., S. L. Gong, T. L. Zhao, R. Arimoto, Y. Q. Wang, and Z. J. Zhou (2003), Sources of Asian dust and role of climate change evrsus desertification in Asian dust emission, *Geophys. Res. Lett.*, *30*(24), 2272, doi:10.1029/2003GL018206.
- Zhang, X. Y., Y. Q. Wang, T. Niu, X. C. Zhang, S. L. Gong, Y. M. Zhang, and J. Y. Sun (2012), Atmospheric aerosol compositions in China: Spatial/temporal variability, chemical signature, regional haze distribution and comparisons with global aerosols, *Atmos. Chem. Phys.*, *12*, 779–799, doi:10.5194/acp-12-779-2012.
- Zhao, C., S. Chen, L. R. Leung, Y. Qian, J. F. Kok, R. A. Zaveri, and J. Huang (2013), Uncertainty in modeling dust mass balance and radiative forcing from size parameterization, *Atmos. Chem. Phys.*, *13*, 10,733–10,753, doi:10.5194/acp-13-10733-2013.
- Zhao, P., R. Zhang, J. Liu, X. Zhou, and J. He (2007), Onset of southwesterly wind over eastern China and associated atmospheric circulation and rainfall, *Clim. Dyn.*, *28*, 797–811, doi:10.1007/s00382-006-0212-y.
- Zhao, T. L., S. L. Gong, X. Y. Zhang, J.-P. Blanchet, I. G. McKendry, and Z. J. Zhou (2006), A simulated climatology of Asian dust aerosol and its trans-pacific transport. Part I: Mean climate and validation, *J. Clim.*, *19*, 88–103, doi:10.1175/JCLI3605.1.
- Zhou, D., et al. (2013), Impacts of the East Asian Monsoon on lower tropospheric ozone over coastal South China, *Environ. Res. Lett.*, *8*, 044011, 7, doi:10.1088/1748-9326/8/4/044011.
- Zhou, L. T. (2011), Impact of East Asian winter monsoon on rainfall over southeastern China and its dynamical process, *Int. J. Climatol.*, *31*, 677–686, doi:10.1002/joc.2101.
- Zhu, J., H. Liao, and J. Li (2012), Increases in aerosol concentrations over eastern China due to the decadal-scale weakening of the East Asian summer monsoon, *Geophys. Res. Lett.*, *39*, L09809, doi:10.1029/2012GL051428.